# THE EFFECT OF LEADING EDGE ROUNDING ON A CARET WAVERIDER CONFIGURATION AT MACH 8.2

**Brian McCartney**[*], **Simon Prince**[*] **& Ning Qin**[+]

[*]**School of Aerospace, Transport and Manufacturing Cranfield University, UK.**
[+]**Faculty of Engineering, University of Sheffield, UK.**

## Abstract

*This paper presents a computational study, with some experimental validation, into the aerodynamic effects of the rounding off of the leading edge of a Caret type waverider at hypersonic speed.*

*The study has confirmed that, at the Mach 8.2 conditions investigated here, the rounding off of the sharp leading edge of a Caret type waverider results in a significant degradation of its lifting capability, both at its design orientation, and at positive angles of attack. Increasing the leading edge radius acts to reduce the lift coefficient, the lift to drag ratio and the pitching moment about the nose, at all angles of attack up to 15°.*

## 1 Introduction

The concept of the waverider configuration, which makes use of the leading edge (LE) shock wave formed during supersonic flight, specifically the high levels of air compression, to generate the aerodynamic lifting force, was first developed by Terence Nonweiler, starting in Belfast in the late 1940s [1]. The requirement is to match the leading edge of the configuration with the shock wave shape in order to trap all of the incoming air between the shock and the body under-surface to maximise the lifting performance [2,3]. Any leakage of flow between the shock wave and the leading edge reduces the lifting performance. Theoretically this means that a sharp LE design, where the shock wave is attached to the leading edge itself, would see no flow leakage.

In practice, however, the thermal loads associated with this shock on sharp leading edge condition is prohibitive, and some level of leading edge rounding, perhaps with active cooling, would be required for a real full-scale hypersonic cruise waverider vehicle.

The work presented in this paper is focused on understanding the level of lift reduction associated with leading edge rounding on the simple Caret style waverider configuration, illustrated in figure 1.

The investigation is limited, in this paper, to a Mach 8.2 Caret configuration, which was matched with one of test Mach numbers available for experimentation in the Cranfield University Hypersonic Gun Tunnel, such that the data obtained in the extensive computational prediction study could be validated with experimental data.
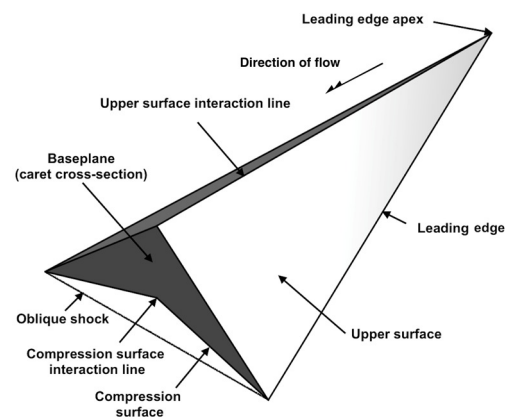


*Fig. 1. Caret waverider concept [1] and associated terminology*

The geometric details of the baseline Mach 8.2 Caret waverider configuration, which has a planform slenderness ratio, $b_{sp}$ = 0.67, are

presented in figure 2a). Two further configurations were developed, one with uniform LE rounding of 8% of the baseline model length, *l*, and the other with twice this level of leading edge rounding, as shown in figure 2.



(a). $r/l = 0\%$ model



(b). $r/l = 8\%$ model



(c). $r/l = 16\%$ model
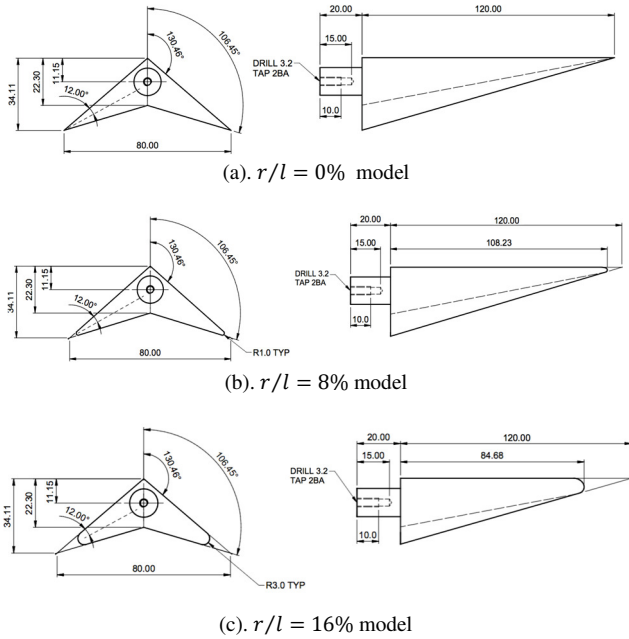
*Fig. 2. Caret waverider half-models (units in mm)*

A detailed computational study was conducted using a Parabolised Navier-Stokes solver, optimised for supersonic and hypersonic flows, for a fixed Mach number of 8.2, with the freestream conditions matching those encountered in the Gun Tunnel experiments. The experimentally validated CFD solutions were then interrogated to reveal the effects of leading edge rounding.

## 2 The Computational Investigation

Numerical simulation was conducted using a structured grid, Implicit Parabolised Navier-Stokes (IMPNS) solver, described by Birch et al. [4], which uses a streamwise marching, finite volume method that assumes that i) the streamwise flow is fully supersonic, except in the inner boundary layers, ii) the stream-wise viscous terms are small and thus may be neglected and iii) the flow is steady. The limitation that no pressure disturbances can propagate upstream means that flow separation is limited to the cross-flow only. The parabolizing approximation of Vigneron et al [5] was employed, whereby a component of the streamwise gradient is neglected.

Calculations were obtained using a 2nd order accurate upwind central differencing scheme to resolve the viscous flow, in the stream-wise direction. In the crossflow plane the inviscid fluxes are calculated using Oshers approximate Riemann solver [6], and the 3rd order Monotonic Upstream-Centered Scheme for Conservation Laws (MUSCL) [7].

The solver employed a multiple-sweep algorithm in the vicinity of the nose of the configuration for the two rounded leading edge cases, where a detached bow shock wave and a very small patch of subsonic flow existed, before the space marching algorithm continued the calculation from the end of the nose radius section.

The IMPNS solver allowed the calculation of laminar and turbulent flow solution, where the Baldwin-Lomax [8], the Degani-Schiff [9] and the Spalart-Allmaras [10] turbulence models were available.

### 2.1 Calculation procedure

#### 2.1.1 Flow Conditions

The freestream flow conditions, which were fixed for all of the calculations, were those of the freestream conditions encountered in the Hypersonic Gun Tunnel experiments, details of which are given in table 1. The ratio of specific heats, γ, is set at 1.4 for perfect air unless otherwise stated.

| | | | |
|---|---|---|---|
| $M_\infty$ | 8.2 | $P_0$ | $10890.6\ kPa$ |
| $Re_\circ$ | $9.01\ x10^6\ m^{-1}$ | $T_\infty$ | $89.3\ K$ |
| $\rho$ | $3.7067\ x10^{-2}\ kg/m^3$ | $T_w$ | $299.15\ K$ |
| $P_\infty$ | $950\ Pa$ | $T_0$ | $1290\ K$ |

*Table 1. Freestream Flow Conditions*

#### 2.1.2 Grids and Grid Convergence

A grid convergence study was performed in order to identify the required level of grid resolution needed to ensure grid insensitivity for

the aerodynamic forces and moments. Table 2 presents the details of the three grids tested.

The percentage deviation from asymptotic values of $C_L$ and $C_D$, excluding base effects, were calculated for the sharp LE model i.e. $r/l = 0\%$ at $M_\infty = 8.2$ and $\alpha = 0°$ from a laminar numerical solution. Using the method by Roach *et al* [11], the Grid Convergence Index (GCI) of 1.591% was obtained for a grid of $88^3$ cells. Details of the CGI obtained for each grid are reproduced in Table 2. A similar study was performed for $\alpha$=10°, yielding similar results and confirming that the fine grid of 681,472 cells was sufficient for the resolution of the aerodynamic characteristic of interest in this study.

| Grid | Cells | $C_L$ | GCI % | $C_D$ | GCI % |
|------|-------|-------|-------|-------|-------|
| Coarse | $44^3$ | 0.046 | - | 0.013 | - |
| Medium | $66^3$ | 0.052 | 1.844 | 0.015 | 1.776 |
| Fine | $88^3$ | 0.049 | 1.798 | 0.014 | 1.591 |

*Table 2. Grid convergence index as established from $C_L$ and $C_D$*

The structured grids comprised two blocks, one covering the flow domain above the waverider, and the other below, with the interface emanating outward from the leading edge, as shown in figure 3, with cell clustering from the body wall (first cell height ~$1\times10^{-6}l$).



*(a). $r/l = 0\%$ model computational domain ($88^3$ cells)*



*(b). $r/l = 8\%$*          *(c). $r/l = 16\%$*
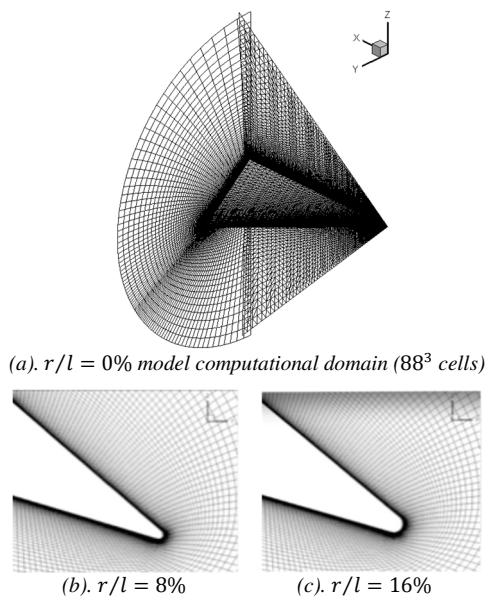
*Fig. 3. The computational structured grids, $88^3$ cells.*

Since only angle of attack was varied in this study, and this is limited to no more than 15°, the flow is expected to be symmetric about the *y*=0 plane, and only half of the domain was computed, with a symmetry boundary condition applied across the *y*=0 faces.

### 2.1.3 Calculation Strategy

Some 2000 initial explicit iterations were computed on each *y-z* crossflow station, before a maximum of 5000 implicit iterations were computed to achieve a target of six levels of residual convergence.

Pitch sweeps were performed for both laminar and turbulent conditions, with angle of attack intervals of 1°, through the range $0° \leq \alpha \leq 10°$, where a theoretical $(L/D)_{max} \approx 5°$ may be expected [2].

## 3 The Experimental Investigation

It was intended to validate the numerical predictions with experimental data from the Cranfield University Hypersonic Gun Tunnel, details of which are provided in reference [12]. The aim was to obtain force and moment and Schlieren flow visualization images (Z-pass arrangement with a Ultima APX 120K high speed camera), under the Mach 8.2 conditions detailed in table 1, where the stabilized run time was ~25*ms*, for the angle of attach range $0° \leq \alpha \leq 10°$.

Unfortunately, the level of model vibration, observed to occur at the end of the stabilized flow period, meant that only data for angles of attack of $\alpha$=0° and $\alpha$=1°, for the *r/l*=0% model could be safely obtained for this paper. A smaller model, of less mass, will be tested later to obtain the complete set of experimental validation data.

Figure 4 compares the experimental Schielren image for $\alpha = 0°$ for the *r/l*=0% model, with the corresponding CFD resolved Mach number contours on the symmetry plane. The agreement in the overall flow structure is good, and the shock-wave on leading edge condition for this angle of attack is confirmed.
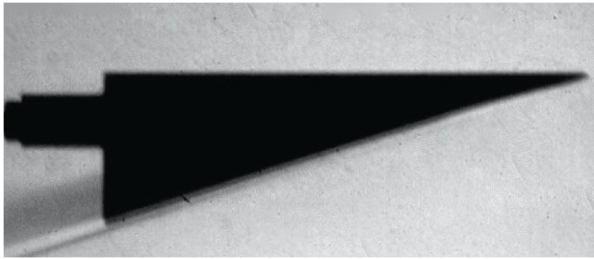
*(a). Schlieren imagery for the baseline model at $\alpha = 0°$*
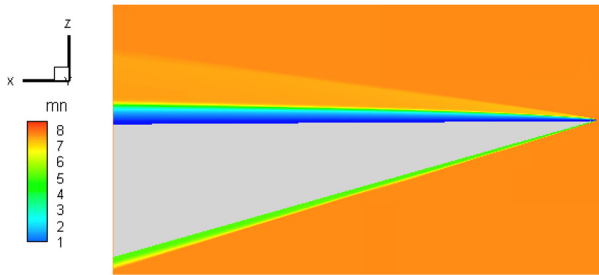


*(b). Contour plot of Mach for the baseline model at $\alpha = 0°$*

*Fig. 4. Numerical validation through Schlieren imagery for the baseline model at $\alpha = 0°$.*
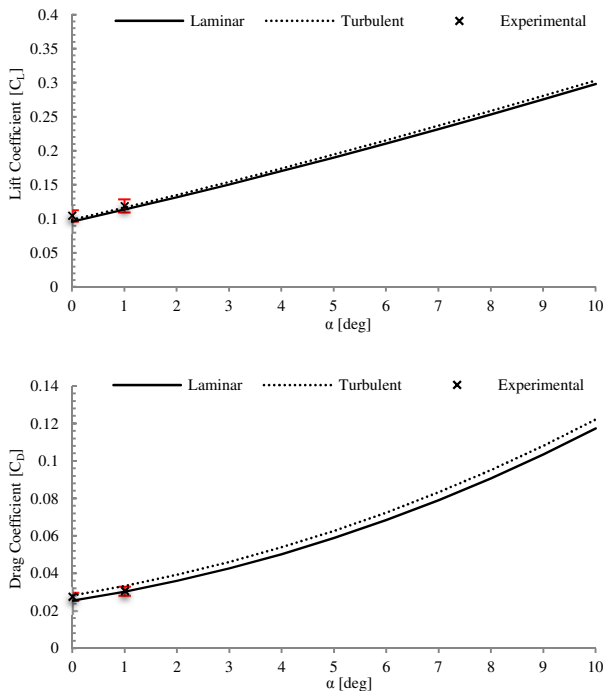




*Fig. 5. Comparison of experimental and CFD resolved forces and moments for the baseline model.*

Figure 5 compares the measured and computed lift and drag coefficient variation with angle of attack for the baseline model. Although only two datapoints are available from the experiments, it is seen that these agree relatively

well with the computed values obtained from IMPNS.

The freestream conditions in the Gun Tunnel suggest that the flow is transitional, and it is interesting to note that the measured values of $C_D$ appear to be between the laminar and turbulent (Spalart-Allmaras in this case) computed values, as would be expected.

The agreement between the available experimental data and the CFD solutions provides some level of confidence that the IMPNS approach is valid and will resolve the correct physical trends. Further validations of this method, and the IMPNS solver in particular, are provided in reference 4.

## 4. Assessment of the Aerodynamic Characteristics of the Baseline Configuration

In addition to the validation of the CFD method with experimental data it was decided to compare the CFD predicted forces and moments with two simple inviscid + skin friction theoretical methods. Simple theory predictions were obtained using exact shock-expansion theory with the addition of viscous effects as calculated using the caret specific method by Rasmussen [13] and the generic method by Eckert [14]. The compression surface was treated as a flat plate with flow deflection angle, $\Delta = 10.5 + \alpha$, and the upper surface as a flat plate with flow expansion angle equal to the angle of attack.

From the theoretical transition location using the method of Sheetz [15], for the $r/l = 0\%$ model, and the skin friction coefficient via the method by van Driest [16] it was predicted that transition was unlikely to occur, under these conditions, within the range $0° \leq \alpha \leq 10°$, and hence laminar skin friction calculations were performed.

Figure 6 presents the comparison of the predicted variation of $C_L$ and $C_D$ with α, using simple theory, with those obtained from IMPNS calculation. The agreement between the two predictions is good at low α, up to around 2º, and is reasonably good up to around 6º for $C_L$. The CFD resolved $C_D$ is significantly higher than the simple theoretical prediction above ~3º. This, in part, is to be expected as the simple

theory takes no account of the drag increment due to the effect of increasing upper surface suction, consistent with the work by Kuester and Anderson [17], and boundary layer displacement.
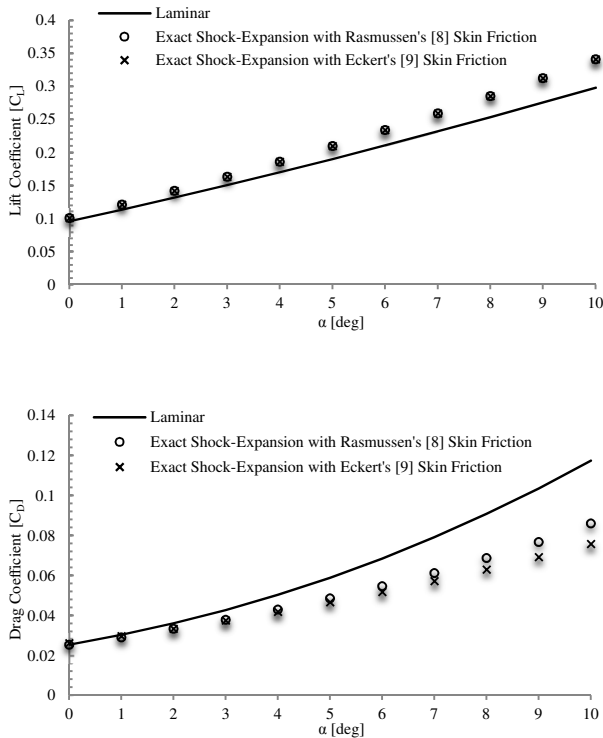




*Fig. 6: Comparison of $C_L$ and $C_D$ versus $\alpha$ for the baseline model, obtained from CFD and those predicted using simple theory.*

Figure 7 plots the corresponding comparison for lift-to-drag ratio, and includes predictions obtained from the theoretical equation for *L/D* ratio for a Caret configuration by Kuchemann [18].

Kuchemann's equation is seen to underpredict the *L/D* level compared with both the CFD prediction and the results of the other theoretical methods, but does capture the same trend, of reducing lift efficiency with $\alpha$, as resolved in the CFD solutions. Conversely, the Shock-Expansion theory based methods both overpredict the *L/D*, and do not predict any significant reduction in *L/D* with $\alpha$.
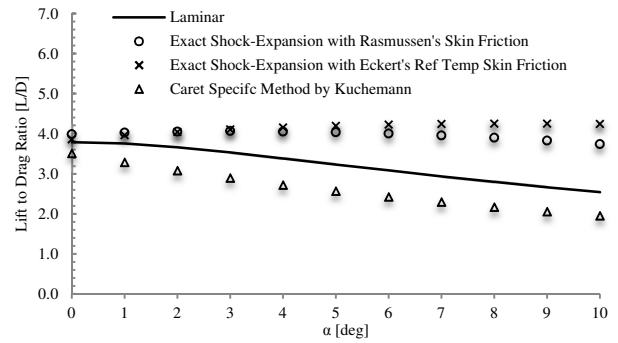


*Fig. 7: Comparison of L/D versus $\alpha$ for the baseline model, obtained from CFD and those predicted using simple theory.*

## 5 The Effect of Leading Edge Rounding

The IMPNS solver was employed to calculate the aerodynamic characteristics of the baseline Caret configuration, and the two configurations with leading edge rounding for the angle of attack range of $0° \leq \alpha \leq 15°$. Since the difference in the predicted forces and moments between all three turbulence models was found to be insignificant, only the Spalart-Allmaras turbulence model results are plotted here.

Figure 8 presents the computed variation of $C_L$ with $\alpha$ for the Mach 8.2 conditions, for the three geometries. There is no discernable difference between the values for laminar and for turbulent flows.
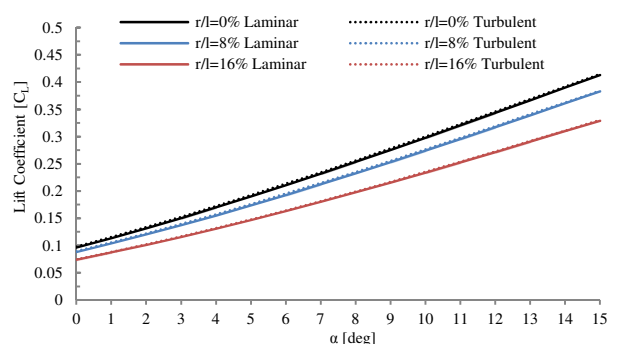


*Fig 8: Effects of LE rounding on $C_L$ for laminar and turbulent calculations, $M_\infty = 8.2$ , $Re = 9.01 \; x10^6 \; m^{-1}$.*

Firstly, the lift curves exhibit only a very small level of non-linearity, which might be expected were significant levels of vortex lift to be present. There is also no evidence of any trend towards stall in any of the lift curves.

The effect of rounding the leading edge on the lift generated is very significant. Rounding with a radius, *r*, of 0.08*l* reduces lift by between 5 – 10% across the whole incidence range. Doubling the rounding radius to 0.16*l* further reduces the lift force coefficient by a further 10 – 20%. Figure 9, which presents the CFD computed pitot pressure contours in the crossflow plane at *x/l* = 0.92, for the laminar condition at α=0°, helps to explain these trends. For the baseline configuration, *r/l*=0, the leading edge shock wave on the underside of the body hits the leading edge apex, as expected, and there is no leakage of the flow through to the upper surface. Introduction of a small level of leading edge rounding allows the shock wave to detach from the leading edge and the lower surface flow to pass around to the upper surface. While the pressure increased locally in the close vicinity of the rounded leading edge, due to the action of the detached shock compression, the effect is an overall reduction in the average pressure experienced by the lower body surface, and an outboard spanwise flow towards the leading edge. For the case of *r/l*=0.16, this spanwise flow is seen to have caused a flow separation, and an incipient vortex in the corner of the lower surface and at the apex of the upper surface.



|  |  |  |
| :---: | :---: | :---: |
| (a). $r/l = 0$ | (b). $r/l = 0.08$ | (c). $r/l = 0.16$ |
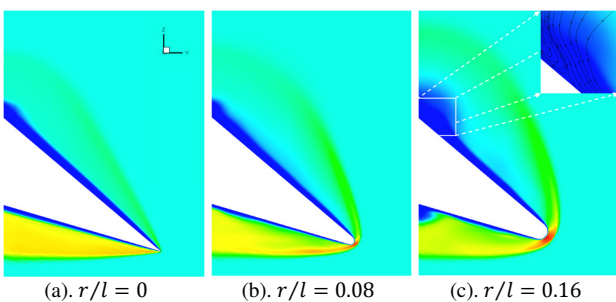
*Fig. 9: Contour plots of pitot pressure in the y-z plane base plane, at x/l=0.92, for laminar CFD solutions at $\alpha = 0°$, $M_\infty = 8.2$, $Re = 9.01\ x10^6\ m^{-1}$.*

The size and strength of the upper surface vortical flow is not expected to contribute significantly to the overall lifting force in this case, and this is consistent with the findings of previous research [19] [20].

Figure 10 presents the corresponding results for the variation of $C_D$ with α. At the design condition (zero α) increasing the extent of LE rounding results in a subsequent increase in total $C_D$. This may be attributed to the increase in wave drag associated with the growing strength of the shock wave near the leading edge, as well as due to the effects of boundary layer separations, and is consistent with previous research [20]. Analysis of the inviscid $C_D$ indicated a 14.59% and 20.06% rise from baseline configuration, for the $r/l = 0.08$ and $r/l = 0.16$ model levels respectively.
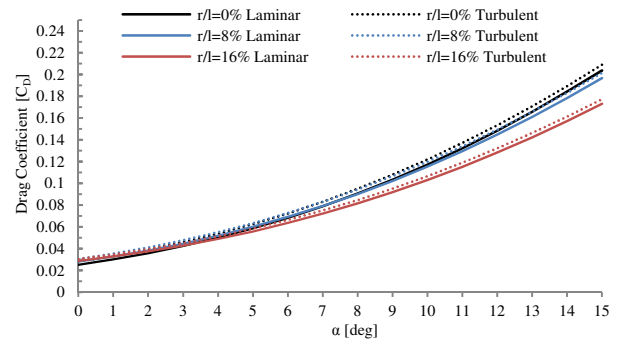


*Fig. 10: Effects of LE rounding on $C_D$ for laminar and turbulent calculations, $M_\infty = 8.2$, $Re = 9.01\ x10^6\ m^{-1}$.*

Below around $\alpha \sim 3°$ the baseline drag is lower than that predicted for both the LE rounded configurations. Above this angle of attack the trend is reversed with the drag coefficient levels for the baseline configuration being highest.

Further investigation identified this as being due to the relative dominance of pressure drag with increasing angle of attack, and the fact that the increased effect of "pressure leakage" from the lower surface to the upper surface results in a lower pressure drag contribution.

The corresponding variation of the pitching moment coefficient, $C_M$, about the nose, is presented in figure 11.
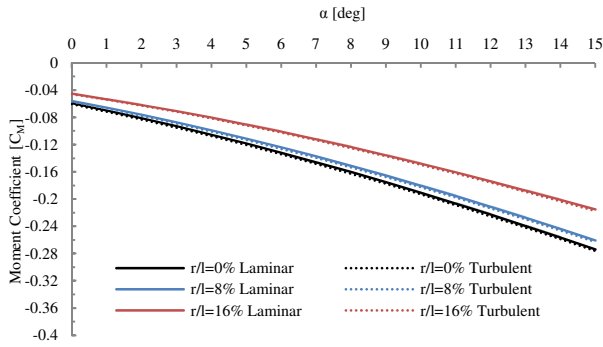
Fig. 11: Effects of LE rounding on $C_M$ for laminar and turbulent calculations, $M_\infty = 8.2$ , $Re = 9.01\ x10^6\ m^{-1}$.

The magnitude of difference in total $C_M$ varies in proportion to the extent of LE rounding, which one may expect given the similar characteristic observed for the total $C_L$. Introduction of leading edge rounding reduces the value of negative $C_M$ at any given angle of attack in the range investigated.

The mean difference in magnitude, Δ, in $C_L$, $C_D$ and $C_M$ from their respective baseline values was established and is presented in Figure 12. The mean differences from $r/l = 0$ model values of the force and moment coefficients indicate that an increase in the extent of LE rounding has significantly greater effects on $C_L$ and $C_M$ compared to that of $C_D$.
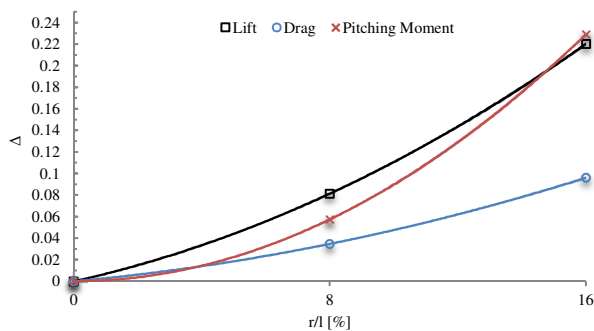


Fig. 12. Mean difference in laminar CFD predicted magnitudes of $C_L$, $C_D$ and $C_M$ with extent LE rounding at $\alpha = 0°$, $M_\infty = 8.2$ , $Re = 9.01\ x10^6\ m^{-1}$.

The trends in the CFD predicted variation of $L/D$ with $\alpha$ were established for laminar and turbulent flows, as illustrated in figure 13. The results indicate, for both laminar and turbulent conditions, that for an increase in extent of LE

rounding there is a corresponding increase in angle of attack at which $(L/D)_{max}$ occurs.

The point of $(L/D)_{max}$ for the $r/l = 0$, 0.08 and 0.16 configurations occurred at an angle of attack of 0°, ~1° and ~2.5° respectively. The data also shows a reduction in the magnitude of $(L/D)_{max}$ of 15% and 27% for the $r/l = 0.08$ and $r/l = 0.16$ models respectively.

Although these reductions are significantly more than analytical approximations for the caret waverider [19], the trends of $L/D$ are in good agreement with previous experimental results for a cone-derived waverider [21], as illustrated in figure 13. This experimental data also confirms that no $L/D$ benefits are realised for the more geometrically complex cone-derived waverider.
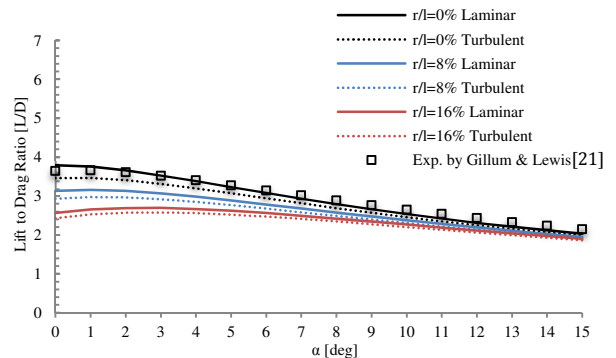


Fig: 13. Effects of LE rounding on $L/D$ for laminar and turbulent calculations, $M_\infty = 8.2$ , $Re = 9.01\ x10^6\ m^{-1}$.

It can also be seen that increasing the leading edge radius progressively reduces the sensitivity of $L/D$ to angle of attack, which is consistent with previous research [22,23].

Analysis of the pressure coefficient, $C_P$, distribution with increasing angle of attack, not illustrated within this document, indicates significant variation over the upper (suction) and lower (compression) surfaces and is most prominent at $(L/D)_{max}$. Specifically, these $C_P$ plots indicate that the drift of the stagnation line from the LE is a result of the upper surface, inward running cross-flow as well as the compression surface pressure leakage at the LE. Furthermore, this stagnation line drift increases with distance downstream for all models and

extent of LE rounding and is indicative of a lifting body with delta planform. The reduction in uniformity of the $C_P$ distribution about the compression surface, with increased LE rounding, is consistent with the findings of previous research [23,24].

To a first order approximation, for $M_\infty = 8.2$, wing sweep angle, $\Lambda = 74.1°$ and corresponding normal Mach, $M_N = 2.25$, the correlations of Stanbrook & Squire [25] suggest that the windward flow over the baseline model may be categorised as having possible shocks and flow expansion over the LE. The CFD predicted flow fields reveal very strong levels of expansion around the leading edge, for all three configurations, at the higher angles of attack. None of the predicted flowfields indicate the formation of any crossflow shock waves above the upper surfaces of the bodies. Figure 14 plots the CFD predicted upper surface skin friction lines for all three models under laminar flow conditions, where the zero angle of attack result is plotted on the left side, and the α=15° result is plotted on the right side in each case. Here, the presence of crossflow shock waves would usually be indicated by the presence of discontinuities in the stream traces. None are seen.



(a). $r/l = 0\%$     (b). $r/l = 8\%$     (c). $r/l = 16\%$
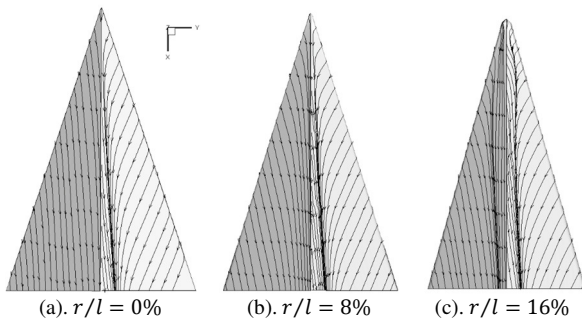
Fig. 14: Laminar computed upper surface streamlines, $\alpha = 0°$ (left side) and $\alpha = 15°$ (right side) for $M_\infty = 8.2$, $Re = 9.01\ x10^6\ m^{-1}$.

Further examination of the upper surface stream traces in Figure 14, reveals attached flow along the LE which may be expected from flow expansion. Furthermore, this figure confirms the presence of inward running cross-flow for all models at $\alpha = 0°$, increasing in magnitude

proportionally with increased LE rounding. For the $r/l = 0.16$ model, at $\alpha = 0°$, this enhanced cross-flow results in the development of a primary separation line.

Also evident in Figure 14, is that increasing the angle of attack to $\alpha = 15°$ increases the angle of the cross-flow, relative to the streamwise component and a primary vortex is generated close to the upper surface apex for all three configurations. This is also illustrated through stream traces plotted in the crossflow contours in figures 15 to 17. For turbulent flow no separations are observed at α=0° while those at α=15° are of much lesser extent than those predicted under laminar conditions.

Figures 15 – 17 present the contours of Mach number on the crossflow plane at $x/l = 0.92$ at angles of attack of 10° and 15° for all three configurations under laminar conditions. In the range $5° \leq \alpha \leq 10°$, the CFD predictions for laminar flow predict the separation and roll up of a relatively strong vortex close to the nose apex of the body which breaks down in the region $\sim x/l = 0.75$. Downstream of this is a large scale viscous region which is left behind, convecting downstream, as seen in the case of figure 17a).

The correlations of Stanbrook & Squire [25], suggest that for a thin wing of similar planform and $r/l = 0$, vortex breakdown should not occur for a wing sweep of $\Lambda = 74.1°$ where $\alpha \leq 25°$. The CFD predictions suggest that leading edge rounding acts to suppress vortex breakdown, though more study is necessary to confirm this.

Increasing the angle of attack to $\alpha = 15°$ significantly increases the strength of the expansion around the leading edge, and results in a strong primary vortex which extends along the whole length of the upper surface, close to the upper surface apex, for all three models. As observed in figures 15 – 17, at this, the highest angle of attack assessed in this study, no strong evidence was found that the leading edge rounding acted to weaken this primary vortex structure. The effect of turbulence was not found to alter the flow structure or the primary vortex strength very much.

| (a). $\alpha = 10°$ | (b). $\alpha = 15°$ |
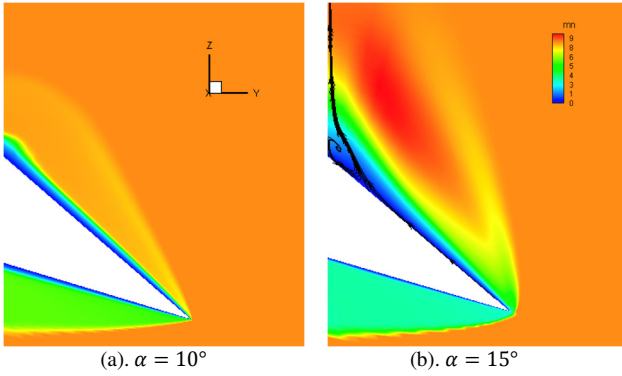
Fig. 15. Contour plots of Mach number at $x/l = 0.92$ in the $y - z$ plane for laminar solutions for the $r/l = 0$ configuration. $M_\infty = 8.2, Re = 9.01 \ x10^6 \ m^{-1}$.



| (a). $\alpha = 10°$ | (b). $\alpha = 15°$ |
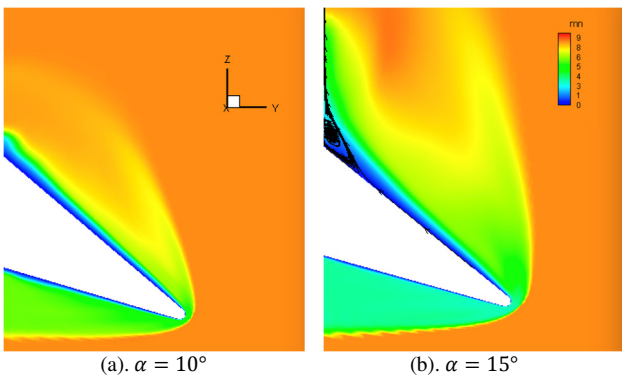
Fig. 16. Contour plots of Mach number at $x/l = 0.92$ in the $y - z$ plane for laminar solutions for the $r/l = 0.08$ configuration. $M_\infty = 8.2, Re = 9.01 \ x10^6 \ m^{-1}$.



| (a). $\alpha = 10°$ | (b). $\alpha = 15°$ |
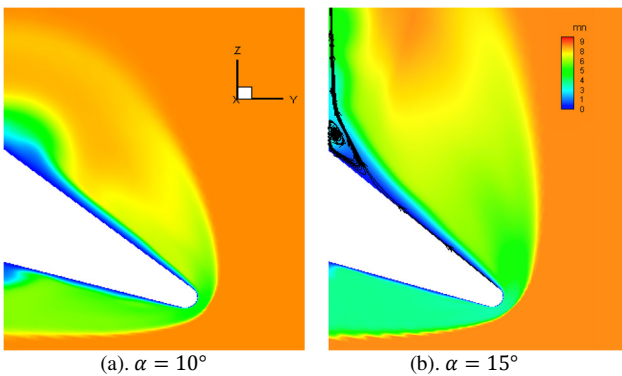
Fig. 17. Contour plots of Mach number at $x/l = 0.92$ in the $y - z$ plane for laminar solutions for the $r/l = 0.16$ configuration. $M_\infty = 8.2, Re = 9.01 \ x10^6 \ m^{-1}$.

## 6 Conclusion

This study has confirmed that, at the Mach 8.2 conditions investigated in this study, the rounding off of the sharp leading edge of a Caret type waverider results in a significant degradation of its lifting capability, both at its design orientation, and at positive angles of attack. Increasing the leading edge radius acts to reduce the lift coefficient, the lift to drag ratio and the pitching moment about the nose, at all angles of attack up to 15°.

## References

[1] Nonweiler, T. R. F., "Aerodynamic problems of manned space vehicles," in *J. Royal Aeronautical Soc.*, vol. 63, pp. 521–528, 1959.

[2] Anderson, J. D. Jr., *Fundamentals of Aerodynamics.*, McGraw-Hill, 5th ed., 2011. ISBN 978-007-128908-5.

[3] Schindler, L. H.,, "Waveriders," in *Tactical Missile Aerodynamics: General Topics,* vol. 141, pp. 321–364, 1992.

[4] T. Birch, S. Prince, D.K. Ludlow and N. Qin, "The application of a parabolised Navier-Stokes solver to some hypersonic flow problems", AIAA Paper 2001-1753.

[5] Vigneron,Y.C., Rakich, J. V., & Tannehill, J. C., "Calculation of Supersonic Viscous Flow Over Delta Wings with Sharp Subsonic Leading Edges", AIAA Paper 78-1137, July 1978.

[6] Osher, S., and Solomon, F. "Upwind difference schemes for hyperbolic conservation laws". *Math. Comp.* vol 38, no 158, pp339-374, 1982

[7] van Leer, B., "Towards the Ultimate Conservative Difference Scheme, V. A Second Order Sequel to Godunov's Method", *J. Comput. Phys.*., vol. 32, pp101–136., 1979.

[8] Baldwin, B., and Lomax, H., "Thin Layer Approximation and Algebraic Model for Separated Turbulent Flow," AIAA Paper 78-257, 1978.

[9] Degani, D., Schiff, L. B, and Levy, Y., "Physical Considerations Governing Computation of Turbulent Flows Over Bodies at Large Incidence," AIAA Paper 90-0096, Jan. 1990.

[10] Spalart, P. R., and Allmaras, S. R., "A one equation turbulence model for aerodynamic flows", *Recherché Aerospatiale*, vol. 1, pp. 5–21, 1994.

[11] Roache, P. J., "Quantification of uncertainty in computational fluid dynamics", *J. Fluid Mech.*, vol. 29, pp. 123–160, 1997.

[12] Needham, D. A.,Elfstrom, G. M., and Stollery, J. L., "Design and operation of the imperial college number 2 hypersonic gun tunnel," Reports 70-04, ICST/AR, 1970.

[13] Rasmussen, M., *Hypersonic Flow*. John Wiley & Sons Inc., 1994. ISBN 0-471-51102-1.

[14] Eckert, E. R. G., "Engineering relations for heat transfer and friction in high-velocity laminar and turbulent boundary-layer flow over surfaces with constant pressure and temperature," *Transactions of the ASME*, vol. 78-6, pp. 1273–1283, 1956.

[15] Sheetz, N. W. Jr., "Ballistic Range boundary-Layer Transition Measurements on Cones at Hypersonic Speeds". *Proceedings of the Symposium on Viscous Drag Reduction* , LTV Research Center, Dallas, Texas, Sept. 24-25, 1968. Springer, 1969.

[16] Van Driest, E, R., "Turbulent boundary layers in compressible fluids", *Journal of the Aeronautical Sciences*, vol. 18, 1951.

[17] Kuester, P. S., and Anderson, J. D. Jr, "Applicability of Newtonian and linear theory to slender hypersonic bodies", *J. Aircraft*, vol. 32(2), pp. 446–449, 1995.

[18] Kuchemann D., "Hypersonic aircraft and their aerodynamic problems", *Prog. Aerospace Sci.*, vol. 6, pp. 271–353, 1965.

[19] Stallings, R. L.,, "Low aspect ratio wings at high angles of attack", *Tactical Missile Aerodynamics: General Topics*, vol. 141, pp. 251–286, 1992.

[20] Collingbourne, J. R., and Peckham, D. H., "The lift and drag characteristics of caret wings at mach numbers between 5 and 10", ARC Report CP 930, RAE, Farnborough, 1966.

[21] Gillum, M. J., and Lewis, M. J., "Experimental results on a mach 14 waverider with blunt leading edges", *J. Aircraft*, vol. 34(3), pp. 296–303, 1997.

[22] Silvester, T. B., and Morgan, R. G., "Computational hypervelocity aerodynamics of a caret waverider", AIAA Paper 2004-3848, 2004.

[23] Liu, J. X.,Hou, Z. X,Ding, G. H.,Chen, X. Q., and Chen, X. Q., "Numerical and experimental study on waverider with blunt leading edge", *J. Computers & Fluids*, vol. 84, 2013.

[24] Townend, L. H, "Research and design for lifting re-entry,", *Prog. Aerospace Sci.*, vol. 18, pp. 1–80, 1979.

[25] Stanbrook, A., and Squire, L. C., "Possible types of flow at swept leading edges", *Aeronautical Quarterly*, vol. 15, pp. 72–82, 1964.

## Contact Author Email Address

For information regarding this research, please contact Brian D. McCartney: brian.mccartney@mbda.co.uk

## Copyright Statement